

See discussions, stats, and author profiles for this publication at: <https://www.researchgate.net/publication/26297445>

Elliptical solitons in nonconventionally biased photorefractive crystals

Article in *Optics Express* · February 2007

DOI: 10.1364/OE.15.000536 · Source: PubMed

CITATIONS

40

READS

68

9 authors, including:



Peng Zhang

Changsha University of Science and Technology

30 PUBLICATIONS 933 CITATIONS

[SEE PROFILE](#)



Cibo Lou

Nankai University

71 PUBLICATIONS 803 CITATIONS

[SEE PROFILE](#)



Jingjun Xu

Nankai University

797 PUBLICATIONS 6,931 CITATIONS

[SEE PROFILE](#)



Zhigang Chen

San Francisco State University

496 PUBLICATIONS 10,865 CITATIONS

[SEE PROFILE](#)

Some of the authors of this publication are also working on these related projects:



Weak Light Nonlinear Optics [View project](#)



Terahertz phonon polariton and its applications: Terahertz integrated chip for sensing, time domain spectroscopy, future communication; and spatiotemporal super-resolution imaging [View project](#)

Elliptical solitons in nonconventionally biased photorefractive crystals

Peng Zhang,¹ Jianlin Zhao,¹ Cibo Lou,² Xiaoyu Tan,^{1*} Yuhan Gao,¹ Qian Liu,¹
Dexing Yang,¹ Jingjun Xu² and Zhigang Chen^{2,3}

¹ Institute of Optical Information Science and Technology, School of Science, Northwestern Polytechnical University, Xi'an 710072, China

² TEDA Applied Physics School, Nankai University, Tianjin 300457, China

³ Department of Physics and Astronomy, San Francisco State University, California 94132, USA

* Present address: Department of Computer Science & Technology, Tsinghua University, Beijing, 100084, China
jlzhao@nwpu.edu.cn

Abstract: We theoretically predict and experimentally observe the two-dimensional (2-D) bright solitons in a nonconventionally biased strontium barium niobate (SBN) crystal. A theory describing light propagating in an SBN crystal with a bias field along an arbitrary direction is formulated. Then the existence of 2-D bright solitons in such a crystal is numerically verified. By employing digital holography, the index changes induced by Gaussian beams in an SBN crystal under different biasing conditions are visualized. Finally, skewed elliptical solitons are experimentally demonstrated.

©2007 Optical Society of America

OCIS codes: (190.5330) Photorefractive nonlinear optics; (190.5530) Pulse propagation and solitons

References and links

1. M. Segev, B. Crosignani, A. Yariv, and B. Fischer, "Spatial solitons in photorefractive media," *Phys. Rev. Lett.* **68**, 923 (1992).
2. G. I. Stegeman and M. Segev, "Optical spatial solitons and their interactions: universality and diversity," *Science* **286**, 1518 (1999).
3. M. Shih, P. Leach, M. Segev, M. H. Garrett, G. Salamo, and G. C. Valley, "Two-dimensional steady-state photorefractive screening solitons," *Opt. Lett.* **21**, 324 (1996).
4. Z. Chen, M. Mitchell, M. Shih, M. Segev, M. H. Garrett, and G. C. Valley, "Steady-state dark photorefractive screening solitons," *Opt. Lett.* **21**, 629 (1996).
5. W. Królkowski and S. A. Holmstrom, "Fusion and birth of spatial solitons upon collision," *Opt. Lett.* **22**, 369 (1997).
6. J. W. Fleischer, M. Segev, N. K. Efremidis, and D. N. Christodoulides, "Observation of two-dimensional discrete solitons in optically induced nonlinear photonic lattices," *Nature* **422**, 147 (2003).
7. J. N. Malmberg, A. H. Carlsson, D. Anderson, M. Lisak, E. A. Ostrovskaya, and Yu. S. Kivshar, "Vector solitons in (2+1) dimensions," *Opt. Lett.* **25**, 643 (2000).
8. Z. Chen, M. Segev, D. W. Wilson, R. E. Muller, and P. D. Maker, "Self-trapping of an optical vortex by use of the bulk photovoltaic effect," *Phys. Rev. Lett.* **78**, 2948 (1997).
9. C. Crognale and L. Rosa, "Vector analysis of the space-charge field in nonconventionally biased photorefractive crystals," *J. Lightwave Technol.* **23**, 2175 (2005).
10. A. Yariv and P. Yeh, *Optical waves in crystals* (Wiley, New York, 1984), Chap. 7.
11. P. Zhang, Y. Ma, J. Zhao, D. X. Yang, and H. Xu, "One-dimensional spatial dark soliton-induced channel waveguides in lithium niobate crystal," *Appl. Opt.* **45**, 2273 (2006).
12. A. A. Zozulya and D. Z. Anderson, "Propagation of an optical beam in a photorefractive medium in the presence of a photogalvanic nonlinearity or an externally applied electric field," *Phys. Rev. A* **51**, 1520 (1995).
13. A. A. Zozulya, D. Z. Anderson, A. V. Mamaev, and M. Saffman, "Solitary attractors and low-order filamentation in anisotropic self-focusing media," *Phys. Rev. A* **57**, 522 (1998).
14. V. I. Petviashvili, "Equation of an extraordinary soliton," *Sov. J. Plasma Phys.* **2**, 257 (1976).
15. J. Zhao, P. Zhang, J. Zhou, D. X. Yang, D. S. Yang, and E. Li, "Visualizations of light-induced refractive index changes in photorefractive crystals employing digital holography," *Chin. Phys. Lett.* **20**, 1748 (2003).
16. E. D. Eugenieva, D. N. Christodoulides, and M. Segev, "Elliptic incoherent solitons in saturable nonlinear media," *Opt. Lett.* **25**, 972 (2000).

1. Introduction

Photorefractive spatial optical solitons have been the topic of extensive research in the past decade due to their physical significance and potential applications in beam steering, optical interconnects, and nonlinear optical devices [1, 2]. It is now well established that photorefractive nonlinearities can support either coherent or incoherent solitons in both transverse dimensions at very low power levels (microwatts and lower), and these solitons can guide a much stronger beam at less photosensitive wavelength. Of particular interest are the so-called screening solitons, which attracted most theoretical and experimental attentions because of the accessibility of self-focusing and self-defocusing in the same crystal simply by reversing the polarity of the bias field and the ease of soliton formations and manipulations, as well as their stability and robustness [2-4]. Nowadays, screening soliton has become a very useful tool in experimental verifications of many predictions of general soliton theory, in particular solitons collision [5] and discrete solitons [6]. Thus far, to our knowledge, the directions of the bias fields for obtaining screening solitons are either parallel (for bright solitons [3]) or antiparallel (for dark solitons [4]) to the c axis of the photorefractive crystal. Then some natural questions arise: What will happen when the bias field is along an arbitrary direction? Can such nonconventionally biased schemes support different types of solitons such as bright, dark, vector [7], vortex [8] and discrete solitons? Will new phenomena appear during soliton formations and their interactions? Recently, space charge fields in nonconventionally biased photorefractive crystals have been numerically analyzed by Crognale and Rosa [9]. In this paper, we theoretically predict and experimentally demonstrate the existence of two-dimensional (2-D) bright elliptical solitons in a nonconventionally biased strontium barium niobate (SBN) crystal.

2. Theoretical analysis

According to the electro-optic effect, for SBN crystals (point group 4mm) with a bias field along an arbitrary direction, it can be easily derived that only the c axis component of the electric field can deform the index ellipsoid remarkably, i.e., contributions introduced by other components can be neglected [10]. This coincides with the fact that light-induced index changes in such crystals are proportional to the c axis components of the space charge fields. Moreover, it should be noticed that only the bias field component perpendicular to the beam propagation direction can result in effective separation of the photo-excited electrons [11]. This implies that, for charge separation, the contribution of an arbitrary bias field is identical to that of its component perpendicular to the beam propagation direction. In general, the essential function of the bias field is to make the photo-excited electrons migrate along a certain direction to form a space charge field. Changing the direction of the bias field may imply altering the orientation of the space charge field. In this case, we can expect different c axis components of the space charge field as well as different distributions of light-induced index changes.

In order to simplify analysis and achieve maximum photorefractive nonlinearity, we consider here a light beam with a polarization direction always parallel to the c axis of the crystal and propagating perpendicular to the c axis. Figure 1 depicts the schematic diagram for a light beam propagating in a nonconventionally biased SBN crystal. The light beam propagates along the z axis, and the direction of the bias field is parallel to the y axis. The angle between the c axis of the crystal and the y axis is denoted as α . According to this geometry, during the process of photorefraction, bias fields will cause photo-excited electrons to drift and separate along the y axis inside the crystal, and this will produce a space-charge field that modulates the index of the material via the electro-optic effect. Corresponding to different α , the c axis components of the fields, which are proportional to the light-induced

index changes, will possess different distributions. Furthermore, these index changes will modulate the propagation of the light beam. If the characteristic spatial scales are larger than the photorefractive Debye length, and the diffusion field can be neglected, the equations determining the steady state propagation of a light beam in a nonconventionally biased SBN crystal can be deduced from the model of Zozulya and Anderson [12, 13]:

$$\left(\frac{\partial}{\partial z} - \frac{i}{2}\nabla^2\right)B(\vec{r}) = i\left(\frac{\partial\varphi}{\partial x}\sin\alpha + \frac{\partial\varphi}{\partial y}\cos\alpha\right)B(\vec{r}) \quad (1a)$$

$$\nabla^2\varphi + \nabla\varphi \cdot \nabla \ln(1 + |B(\vec{r})|^2) = \frac{\partial}{\partial y} \ln(1 + |B(\vec{r})|^2) \quad (1b)$$

where $\nabla = \hat{x}(\partial/\partial x) + \hat{y}(\partial/\partial y)$, $B(\vec{r})$ is the amplitude of the optical field, and φ is the light-induced dimensionless electrostatic potential with the boundary condition $\nabla\varphi(\vec{r} \rightarrow \infty) \rightarrow 0$. The dimensionless coordinates (x, y, z) are related to the physical coordinates (x', y', z') by the expressions $(x, y) = (kl)^{1/2}(x', y')$ and $z = lz'$, where $l = 0.5k^2n_e^2\gamma_{33}E_0$. Here, k is the wave number of light in the crystal, n_e is the extraordinary refractive index, γ_{33} is the electro-optic coefficient, and E_0 is the amplitude of the external field.

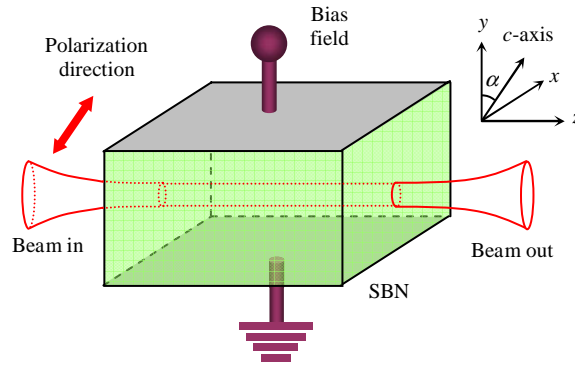


Fig. 1. Geometry of light beam propagation in a nonconventionally biased SBN crystal.

3. Nonlinear index changes and beam propagation

Numerical solutions of Eqs. (1) for an input beam $B(\vec{r}) = \sqrt{2} \exp[-(x^2 + y^2)/16]$ and different values of α are shown in Fig. 2, where the normalized index changes are equal to $\frac{\partial\varphi}{\partial x}\sin\alpha + \frac{\partial\varphi}{\partial y}\cos\alpha$, and the display areas are all 55×55 . Figures 2(a) and 2(b) describe the profiles of the input beam and the linearly diffracted beam with a normalized propagation length $z=15$, respectively. The electrostatic potential induced by the input beam is shown in Fig. 2(c), where the orientation of the c axis and the color index are both indicated. It is obvious that the potential is symmetric to the y axis but not to the c axis. This is because the photo-excited electrons have been drifted parallel to the bias field. Figures 2(d)-(h) depict the simulation results for $\alpha=0, \pi/4, \pi/2, 3\pi/4, \pi$, respectively, where from top to bottom they display index changes induced by the same input beam [see Fig. 2(a)], the output beams after nonlinear propagations, and the corresponding nonlinear index changes at $z=15$. Recall that, as α changing, the polarization directions of the beams are always parallel to the c -axis. It is revealed that the maximum index change at $\alpha=0$ (the largest) is about three times as large as that at $\alpha=\pi/2$ (the smallest), which cannot be seen from the figures as the color is normalized. From Figs. 2(d)-(h) we can see that different biased fields will cause different index changes as well as various nonlinear beam propagations. With α increasing from 0 to π , the crystal is gradually converted from a self-focusing medium into a self-defocusing medium, and the

critical point is at $\alpha=\pi/2$. Similar results are obtained for the case with $\alpha<0$ due to the symmetries of Eqs. (1). From Figs. 2(e₃) and (f₃), it is obvious that such index changes may support 2-D elliptical bright solitons. So in the nonconventional biased SBN crystal, where bright solitons exist, the corresponding α must lie in the interval $[-\pi/2, \pi/2]$.

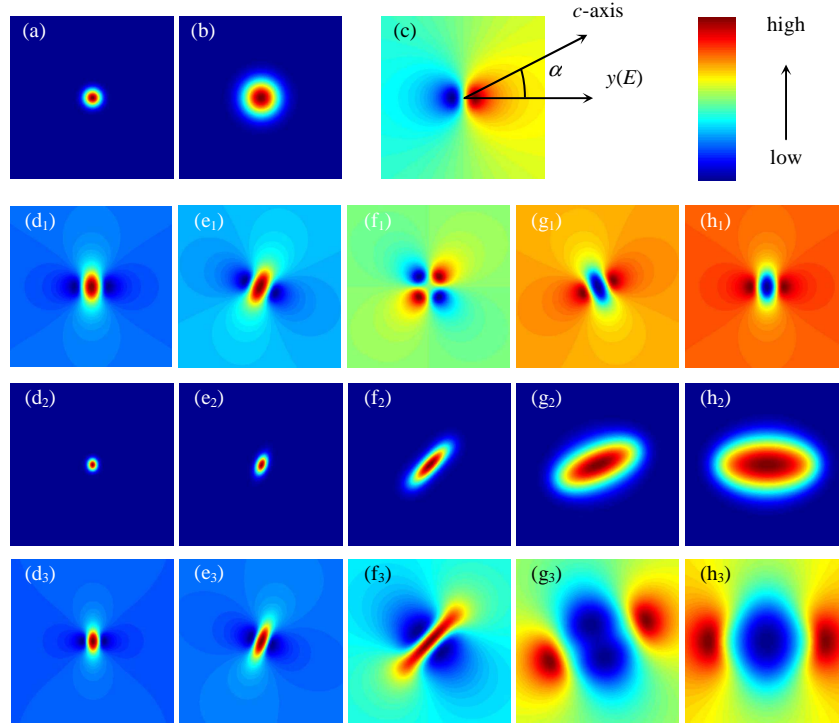


Fig. 2. Numerical simulations of the index changes and beam propagations in a nonconventionally biased SBN crystal. (a) Input beam; (b) Linearly diffracted beam; (c) Light-induced potential; (d)-(h) Index changes induced by the input beam shown in (a) (top), output beams after nonlinear propagations (middle), and the corresponding nonlinear index changes at $z=15$ (bottom) for the cases of $\alpha=0, \pi/4, \pi/2, 3\pi/4$, and π , respectively.

4. Soliton solution and its properties

Now, we seek solitary solutions of the system of Eqs. (1) in the standard form $B(x, y, z)=b(x, y)\exp(i\beta z)$, where β is the propagation constant, and the real envelope $b(x, y)$ satisfies the following equations

$$\left(\beta - \frac{1}{2}\nabla^2\right)b(x, y) = \left(\frac{\partial\varphi}{\partial x}\sin\alpha + \frac{\partial\varphi}{\partial y}\cos\alpha\right)b(x, y) \quad (2a)$$

$$\nabla^2\varphi + \nabla\varphi \cdot \nabla \ln(1 + |b(x, y)|^2) = \frac{\partial}{\partial y} \ln(1 + |b(x, y)|^2) \quad (2b)$$

We numerically solve the eigenproblem Eqs. (2) by employing the renormalized iterative procedure due to Petviashvili [14]. Setting $\alpha=0$, we derive the same results as that presented in Ref. [13]. Here, our purpose is to deal with the cases with $\alpha\neq 0$, i.e. the nonconventionally biased scheme. It is found that 2-D bright elliptical solitons indeed exist in a nonconventional biased SBN crystal. The simulation results are shown in Fig. 3, where from the first to the third row they correspond to the results for $\alpha=0, \pi/4$ and $\pi/2$, respectively, and the

corresponding display areas are 40×40 , 40×40 , and 75×75 . Figures 3(a)-(c) depict soliton solutions for different propagation constant β . Figures 3(d) depict the index changes induced by the solitons corresponding to Figs. 3(b). Figure 3(e) shows the soliton maximum intensity I_{\max} versus the propagation constant β for the cases of $\alpha=0$, $\pi/8$, $\pi/4$, $3\pi/8$, and $\pi/2$, respectively. The full width at half maximum (FWHM) of the soliton intensity profile W_1 and W_2 , which are corresponding to the two principal axes of the ellipse and are indicated in Figs. 3(a), and the ratio W_1/W_2 versus I_{\max} are shown in Fig. 3(f). From Fig. 3, we can see that for the nonconventionally biased case the soliton profiles are also elliptical. However, the orientations of the ellipses are skewed due to the tilted bias fields. When $\alpha > \pi/4$, the ranges of the eigenvalues β for the existed solitons will reduce fast with increasing α . Moreover the convergence speed of the iterative procedure becomes slower. For this reason, the maximum eigenvalues β in our calculation for the cases of $\alpha=3\pi/8$ and $\pi/2$ are 0.35 and 0.18, respectively. For the case $\alpha=\pi/2$ as well as the external field is biased perpendicular to the c axis of the crystal, to observe solitons in experiment, the ratio between the soliton and the background beam intensities, i.e. I_{\max} , cannot be too large because of the dramatically increase of W_1/W_2 after I_{\max} becomes larger than 2.

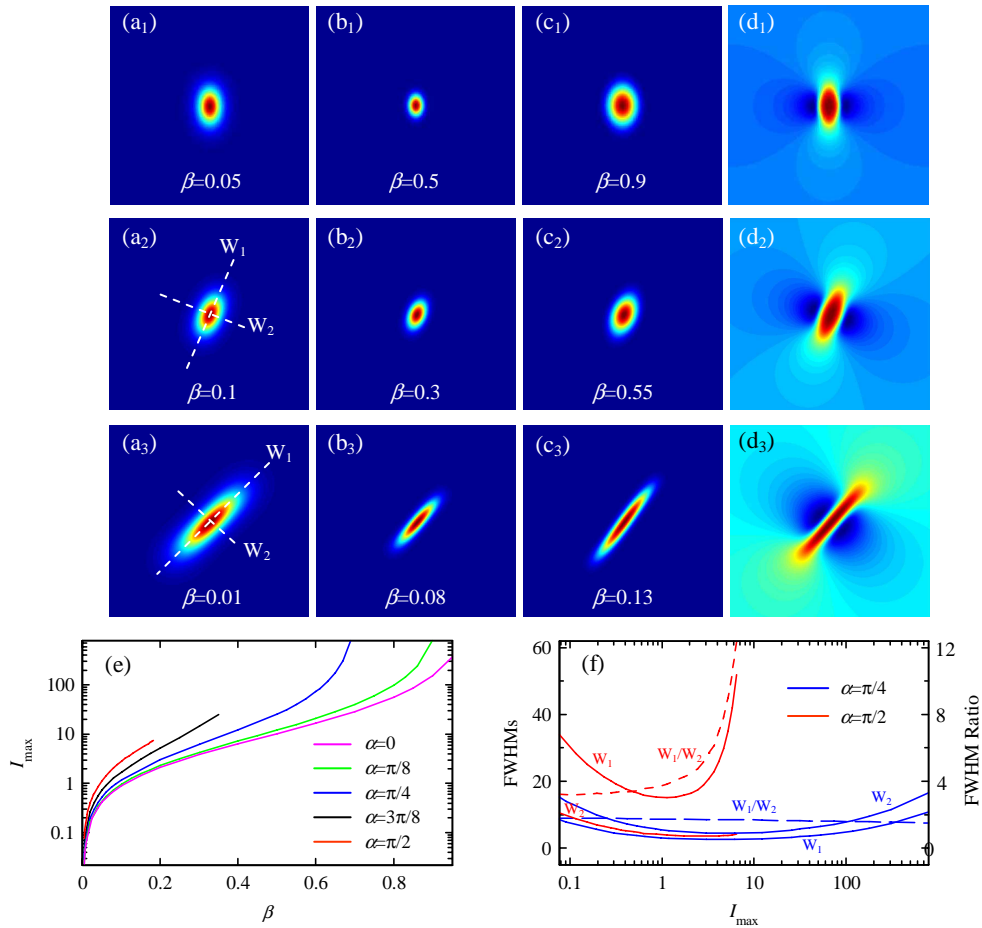


Fig. 3 Simulation results for 2-D bright elliptical solitons in nonconventionally biased SBN crystal. (a)-(c) Solitons with different propagation constant β ; (d) Index changes induced by the solitons shown in (b); From the first to the third row, they are the results for $\alpha=0$, $\pi/4$ and $\pi/2$, respectively. (e) Soliton maximum intensity I_{\max} versus β ; (f) FWHMs of the solitons and their ratio versus I_{\max} .

5. Soliton excitation by Gaussian beams

When we substitute the soliton solutions into Eqs. (1) to check the evolutions of the beam profiles, it is found that the profiles do not change during propagation as expected. However to observe the soliton formations in experiment, a Gaussian beam with circular symmetry are usually used. Could circular Gaussian beams evolve into elliptical solitons in a nonconventionally biased photorefractive crystal? To answer this question, some numerical simulations are performed. Figure 4 describes the linear and nonlinear evolutions of the input Gaussian beam $B(\vec{r}) = \sqrt{1.6} \exp[-(x^2 + y^2)/36]$ in an SBN crystal with a bias field perpendicular to the c axis, where the display areas for (a)-(o) are 400×400 . Figures 4(a)-(e) shows the linear diffracted beam profiles at propagation lengths $z=0, 150, 300, 450,$ and 600 , respectively, while Figs. 4(f)-(j) and Figs. 4(k)-(o) describe the beam profiles and their induced index changes after nonlinear propagations with $z=50, 100, 300, 450, 600$, respectively. Figure 4(p) shows the FWHMs of the beam profiles along the dashed lines indicated in Fig. 4(a) and (f) versus the propagation lengths z . Here, we also use W_1 and W_2 to denote the FWHMs of the long and short axes of the elliptical beam profiles. From these

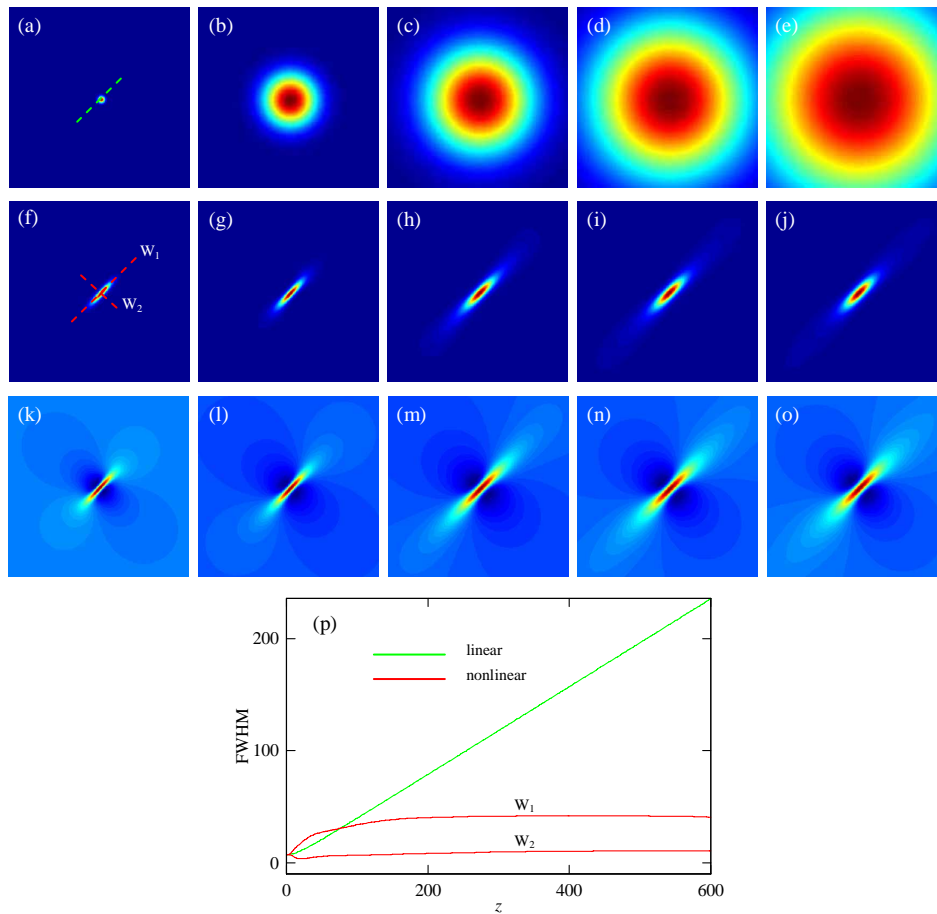


Fig. 4. Simulations of the evolutions of a Gaussian beam in a nonconventionally biased SBN crystal. (a)-(e) Linear diffracted profiles with $z=0, 150, 300, 450, 600$, respectively; (f)-(j) Beam profiles after nonlinear propagated with $z=50, 100, 300, 450, 600$, respectively; (k)-(o) Nonlinear index changes corresponding to the beam profiles in (f)-(j); (p) FWHMs of the beams versus propagation lengths z .
(2.28 MB) Movie of the evolutions of linear diffraction, nonlinear propagation, nonlinear index changes, and the FWHM of a Gaussian beam in a nonconventionally biased SBN crystal.

results we can see that a circular Gaussian beam indeed can evolve into a soliton in a nonconventionally biased SBN crystal. And it is also revealed that only the Gaussian beams with proper beam diameters and I_{\max} can evolve into solitons, otherwise the spatial evolution of the input Gaussian beam will experience oscillations similar to that shown in Ref. [13].

6. Experimental demonstration

To perform experimental demonstrations, an SBN:60 crystal with dimensions of 6.5mm×6.5mm×6.7(c)mm and 0.025% by weight chromium dopant is used. We first visualize the index changes induced by a Gaussian beam in a nonconventionally biased SBN crystal employing digital holography. The experimental setup is as same as that described earlier in Ref. [15]. A thin laser beam emitted from a He-Ne laser with wavelength of 633nm is employed to introduce index changes according to the geometry shown in Fig. 1. And the diameter of the writing beam is about 0.2mm and the power density is about 10mW/cm². After the crystal sample is illuminated for 3s without any background beam, the measured index changes are depicted in Fig. 5, where (a)-(d) are the 2-D maps of the index changes for $\alpha=0, \pi, \pi/2$ and $-\pi/2$, respectively, and (e) is the 3-D display of (d). For obtaining Figs. 5(a) and 5(b), the amplitudes of the bias voltages are all 1kV, and in this case the maximum index changes are all about 1.5×10^{-4} . For obtaining Figs. 5(c) and 5(d), bias voltages of 2kV are applied. In this case the maximum index changes are all about 3×10^{-5} . It is obvious that although a higher bias field is applied perpendicular to the c axis, the maximum index changes are much smaller than that in conventionally biased case. This is due to the differences between the amplitudes of the two vertical components of the light-induced electric fields (see numerically simulated results in Fig. 2).

For observing soliton formations, the experimental setup is shown in Fig. 6. A thin He-Ne laser beam is directly focused onto the crystal front face by lens L_1 ($f=15$ cm), and the beam profile at the rear face is monitored by a CCD camera through imaging lens L_2 ($f=5$ cm). The bias field can be applied onto the crystal parallel or perpendicular to the c axis. A cold white light source is used to provide an incoherent background illumination. The total intensity of the He-Ne laser impinging onto the crystal is reduced to about 5 μ W and the intensity ratio between the soliton beam and the background beam can be adjusted by the white light source. Figure 7 shows the experimental results, where (a) is the beam profile of the input Gaussian beam (FWHM is 22 μ m) for generating solitons, (b) is the beam profile (FWHM is 42 μ m) on the rear face of the crystal after linear diffraction. Figures 7(c) and (d) are the soliton profiles under 3.6kV bias voltage with $\alpha=\pi/2$ (in this case $W_1=46\mu\text{m}$ and $W_2=14\mu\text{m}$) and $\alpha=-\pi/2$ (in this case $W_1=46\mu\text{m}$ and $W_2=13\mu\text{m}$), respectively. Figures 7(e)-(h) display the beam profiles observed on the rear face of the crystal with bias voltages of 1kV, 2kV, 3kV, and 3.8kV,

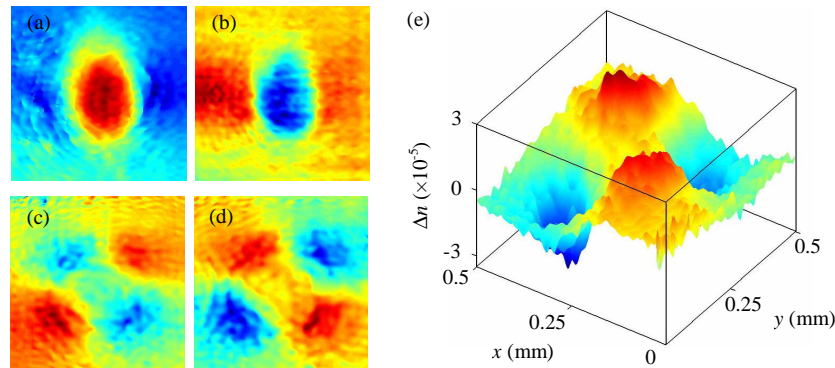


Fig. 5. Measured light-induced index changes in a nonconventionally biased SBN:Cr crystal. (a)-(d) 2-D maps of index changes for $\alpha=0, \pi, \pi/2$ and $-\pi/2$, respectively; (e) 3-D display of (d).

respectively. And the normalized intensities with respect to the background illuminations for Figs. 7(c)-(h) are always adjusted to be about 1. It can be seen that, with the increase of the voltage, the FWHM of the short principal axis of the elliptical beam profile (W_2) is reduced from $31\mu\text{m}$ to $13\mu\text{m}$, while the long one (W_1) is increased from $40\mu\text{m}$ to $45\mu\text{m}$. The ratios W_1/W_2 for the elliptical soliton profiles shown in Figs. 7(c), (d), and (h) are about 3.29, 3.54, and 3.46, respectively, which are approximately the theoretically expected values. Figures 7(i)-(l) display the output beam profiles with bias voltage of 3.6kV , and with normalized intensities of 2, 1.3, 0.8, 0.6, respectively. Combining with Fig. 7(c), it is clear that the FWHM of the output beam has a minimum at normalized intensity of about 1, and with increase or decrease of the normalized intensity, the input Gaussian beam cannot convergences into a soliton, which coincide with the theoretical expectation.

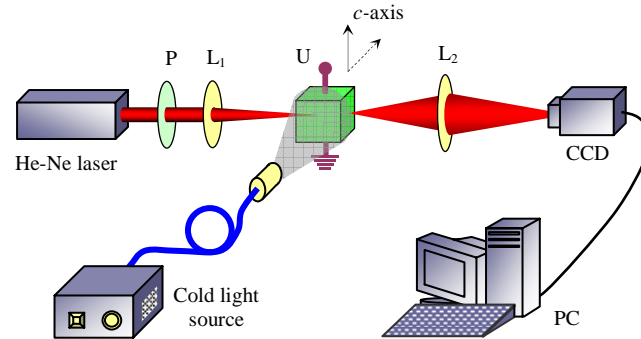


Fig. 6. Sketch of the experimental setup for observing bright solitons in nonconventionally biased SBN crystal.

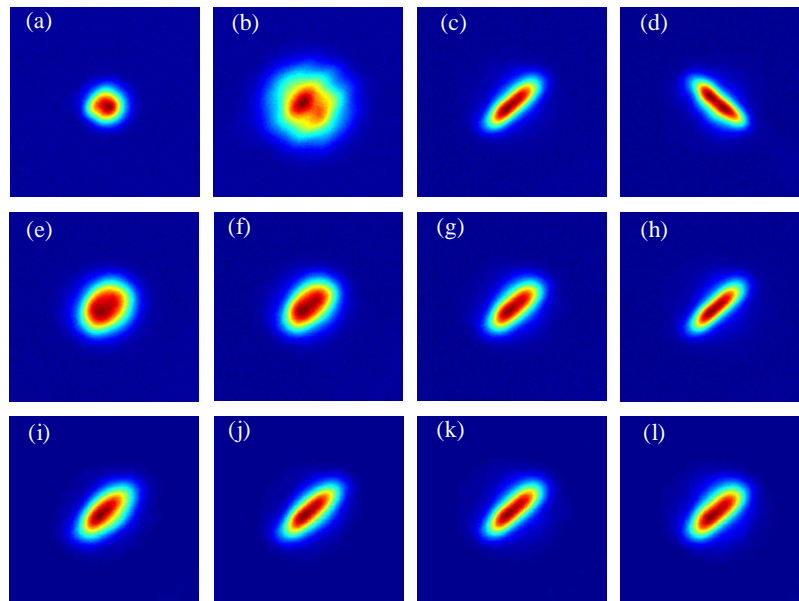


Fig. 7. Experimental results for observing soliton formations in a nonconventionally biased SBN:Cr crystal. (a) Profile of input Gaussian beam; (b)-(d) Beam profiles observed on the rear face of the crystal for a linearly diffracted beam, and the solitons formed with $\alpha=\pi/2$ and $-\pi/2$, respectively; (e)-(h) Output beam profiles as the bias field is increased gradually; (i)-(l) Output beam profiles as the background beam illumination is increased gradually.

7. Summary

In summary, we have formulated a theory describing light propagating in a nonconventionally biased SBN crystal, based on which light-induced index changes and the space evolutions of Gaussian beams have been simulated. The existence of 2-D bright elliptical solitons in an SBN crystal with nonconventional biased scheme has been numerically verified. By employing digital holography, the index changes induced by a Gaussian beam in an SBN crystal under different biasing conditions are visualized. 2-D bright elliptical solitons in an SBN crystal with a bias field perpendicular to the c axis of the crystal are experimentally observed. The experiments are in agreement with the theoretical predictions. It is clear that bias fields along different directions can support 2-D bright solitons. These solitons are just like those formed in conventionally biased crystals except that they are elliptical and they have different orientations. While it is not surprising that elliptical spatial solitons can be generated with anisotropic nonlinearity or anisotropic correlation functions as in elliptical incoherent solitons [16, 17], our scheme with nonconventionally biased photorefractive crystals provides a convenient way for generating such elliptical solitons. We expect different type of elliptical solitons such as vector, vortex, and discrete solitons along with their interactions can be observed in nonconventionally biased photorefractive crystals, where soliton ellipticity may lead to new features not available to circular solitons.

Acknowledgments

The authors thank R. Pankrath and S. Kapphan in University of Osnabrück for providing crystal samples, Jianke Yang in University of Vermont and Romano A. Rupp in University of Vienna for helpful discussions. This work was supported by the National Natural Science Foundation of China, the Youth for Northwestern Polytechnical University (NPU) Teachers Scientific and Technological Innovation Foundation, and the Doctorate Foundation of NPU.